Neutron-Imaging Instrument CONRAD

Nikolay Kardjilov, André Hilger, Ingo Manke, Markus Strobl,
Martin Dawson, and John Banhart
Helmholtz-Zentrum Berlin für Materialien und Energie, Berlin, Germany

Introduction

Conventional neutron imaging is based on the mapping of the attenuation function for a sample in a neutron beam. The intensity map obtained can be represented as an image with two main parameters: spatial resolution and contrast. The spatial resolution is influenced by the beam definition (collimation) and the detector system, whereas the contrast is governed by the interaction of the neutrons with matter, i.e. through absorption and scattering in the sample.

Neutron tomography enables investigations of the macroscopic internal structures of large samples (up to hundreds of cubic centimeters) with a spatial resolution of up to 50 µm. The neutron beam can pass through centimeters of metal but it is easily attenuated by small amounts of light elements like hydrogen, boron and lithium. This makes neutron tomography a unique tool for non-destructive testing with applications in industry, materials science and various other fields. Examples for industrial applications are quality tests of soot filters, adhesive joints, lubricate films and *in situ* visualization of water management in fuel cells.

Instrumentation

Motivated by the high potential of neutron tomography, the Helmholtz-Zentrum Berlin (HZB), Germany, set up the facility CONRAD (Cold Neutron RADiography). It was built providing high flexibility for different kinds of radiographic and tomographic measurements in order to meet the needs of high-flux applications such as real-time imaging and high-speed tomography as well as high-resolution applications.

CONRAD at HZB is located at the end of the curved neutron guide NG1b facing the cold source of the BER-II reactor [1]. The cold-neutron flux density at the end of the guide is of the order of 2×10^8 n/cm^{2}s with a negligible fraction of gammas and fast neutrons. CONRAD includes two measuring positions. The first position is located directly at the end of the neutron guide, taking advantage of the high neutron-flux density available at this position, also required for performing unique real-time experiments and high-speed tomography. However, poor beam-collimation of the guide limits the spatial resolution, and the beam size is defined by the cross-section of the guide, which is 3×12 cm^2.

The second measuring position uses point-source geometry in order to increase the image resolution. For this purpose an additional collimation system, consisting of a flight tube of 5 m length and a set of diaphragms, is installed. This way the collimation ratio defined as pinhole-to-detector path length over aperture diameter (L/D) can be increased to about 500–1000. A pinhole exchanger with 4 circular apertures (diameters of 5, 10, 20 and 30 mm) allows choosing

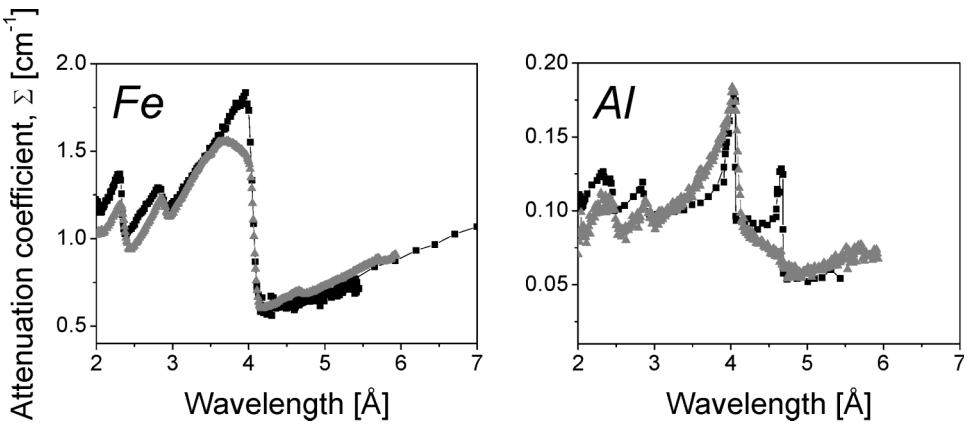

Figure 1. Tabulated (dark, ■) and radiographically (light, ▲) measured attenuation coefficients of Fe and Al using a double-crystal monochromator device, equipped with PGCs having mosaicity of 0.8°.

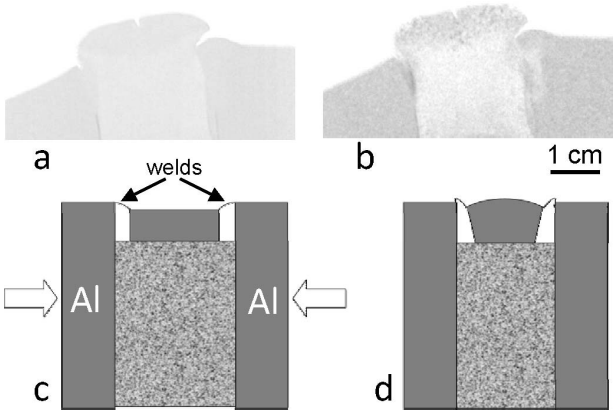

Figure 2. AFS material visualized by a) a white neutron beam and b) a monochromatic beam at 4.6 Å. The container filled with aluminium foam c) is pressed uni-axially and later rolled to form the sandwich structure d) [3].

the optimal L/D ratio and for corresponding measurements. The maximum spatial resolution achieved at that position is 50 µm. The detector system used is based on a 16-bit cooled CCD camera (Andor DW436N-BV) with 2048 × 2048 pixels. The beam size at the second position is approximately $10 \times 10\,cm^2$.

As part of HZB's upgrade program for cold-neutron instrumentation (see separate article in the present issue), CONRAD's flight path will be increased to 10–12 m providing a larger beam size (field of view) of $20 \times 20\,cm^2$ with higher neutron-flux density due to the new neutron guides with super-mirror coating.

The first 3 years of operation proved the important role of neutron imaging at HZB with a beam-time demand approximately twice as high as beam time available. Using the unique, non-destructive neutron tomography technique, HZB users investigated a broad spectrum of applications related to materials science, engineering and fundamental physics, because CONRAD combines applied and fundamental research activities; highlights are given below.

Energy-selective radiography

The neutron attenuation coefficient for polycrystalline materials decreases suddenly (i.e. the transmitted intensity increases sharply) for well-defined neutron wavelengths – the so-called Bragg edges [2]. The position of these edges is defined by the symmetry and the parameters of the crystal lattice. At wavelengths longer than this critical value no scattering by particular {h k l} lattice spacings can occur because the corresponding Bragg reflection angle reaches its maximum of $2\theta = 180°$.

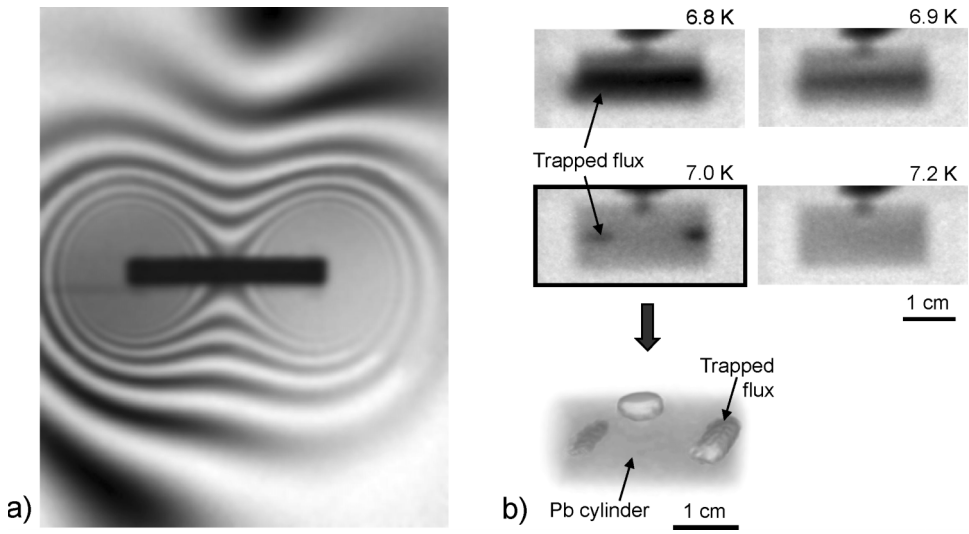

Figure 3. a) A radiograph showing the "field lines" surrounding a dipole magnet. The magnetic field decreases with increasing distance from the magnet, resulting in a series of maxima and minima, where the beam polarization is sequentially parallel or anti-parallel, respectively, to the analyzer. Very close to the magnet (where the field is strongest), the lines are too close together to be resolved spatially. b) A three-dimensional reconstruction of residual flux inside a polycrystalline lead cylinder. When cooled to below its critical temperature in the presence of a weak magnetic field, some flux is trapped inside due to defects and grain boundaries even when the external field has been switched off [8].

Quantitative measurements around Bragg cut-offs for Fe and Al were performed with monochromatic neutrons by using a double-crystal monochromator [3,4] and were compared with tabulated values. Fig. 1 shows the deviation from the tabulated values that can be explained by texture orientations in polycrystalline materials [5].

The imaging technique with monochromatic neutrons can be used to tune the contrast in radiographs. The position of the Bragg-cut-offs can be related to the correspondent d_{hkl} spacing. The height of the Bragg cut-off is reciprocal to the number of crystallites having a defined orientation, which means that information about the distribution of texture fields in the sample can be extracted by studying its shape [6,7].

In order to test this method an Aluminium Foam Sandwich (AFS) precursor material of 10 mm thickness has been measured radiographically with a white beam (Fig. 2, left) and at a wavelength of 4.6 Å – close to the Bragg cut-off for aluminium [3]. The lack of contrast in Fig. 2a is due to the uniform thickness of the sample and the homogeneous material composition. The image at a defined neutron wavelength shows contrast due to the coherent Bragg scattering. The dark areas in Fig. 2b can be related to crystallites having the same orientation to the incident beam. Their formation can be explained by the manufacturing process illustrated in Fig. 2c, d. An aluminium container consisting of welded plates is filled with Al foam precursor, Fig. 2c. After foaming the container is pressed uni-axially and a sandwich structure is produced by rolling, see Fig. 2d. Due to the high temperature at welding and high pressure at rolling, recrystallization in the aluminium plates is possible.

Spin-polarized neutron imaging

Polarized neutron radiography is based on the spatially resolved measurement of the final precession angles of a collimated and polarized monochromatic neutron beam that transmits a magnetic field present inside and outside a sample [8–10]. For this purpose the instrument CONRAD was equipped with solid-state polarizing benders [11] using the double-crystal monochromator device [3,4] for selecting a defined wavelength. The achieved spatial resolution in the radiography images was around 500 µm for the given experimental geometry.

The potential of the method was demonstrated by visualization of the magnetic field around a (dipole) bar magnet, Fig. 3a. In some cases the method can also be extended into three dimensions by a standard tomographic technique, as indicated in Fig. 3b showing the distribution of a magnetic field trapped inside a lead cylinder and becoming superconductive when cooled below its critical temperature at 7.2 K.

Visualizing fuel-cell operation

Neutron radiography is a powerful tool for visualization and quantification of water distribution and transport in complicated devices like fuel cells [12], because neutrons

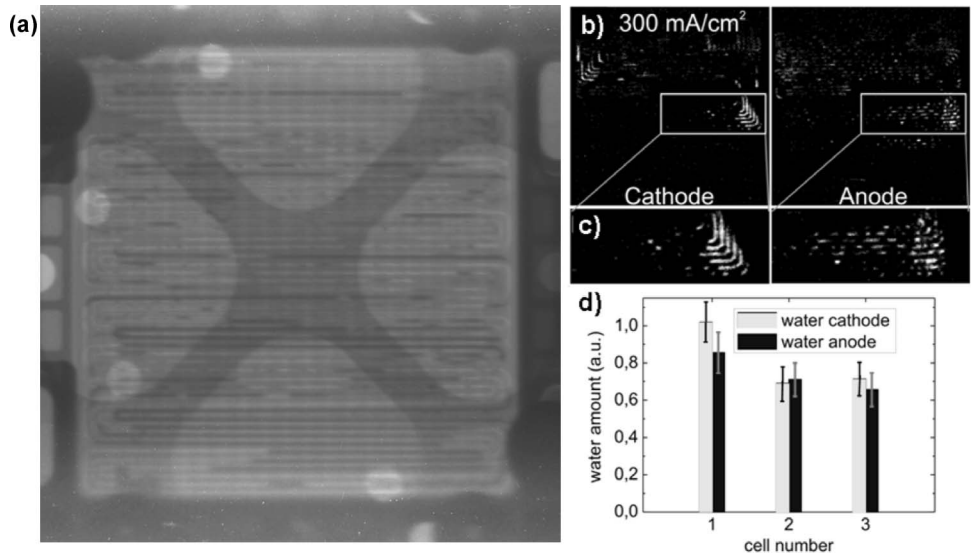

Figure 4. a) Neutron radiographic image of operating Polymer Electrolyte Membrane fuel cells (active area 10 × 10 cm^2). The water accumulation in the flow field channels can be seen as dark lines. b) Water distributions in the anodic (left) and cathodic (right) flow field channels of the first cell in a triple fuel-cell stack (j_0 = 300 mA/cm^2); c) details corresponding to the marked areas in (b). d) Total water content in the anodic and cathodic flow fields of all three cells at j_0 = 300 mA/cm^2 [12].

provide a high sensitivity for the detection of water in a metal matrix. While the metal layers can be penetrated relatively easily, the probability for the interaction of a neutron with hydrogen and all hydrogen-containing materials is high. Therefore, strongly different attenuation coefficients of the metal matrix and the water inside enable a high contrast even for small water quantities in, e.g., metal assemblies. The electrochemical reaction of hydrogen with oxygen in a fuel cell produces water, an essential aspect of fuel-cell operation. Used simultaneously with other advanced, spatially resolved characterization methods of the cells' electrochemistry, neutron tomography provides important insights into fuel-cell operation as shown in Fig. 4, distinguishing between the water distribution on the cathodic and anodic side [12].

Water uptake in plants

Water uptake and water transport in plants are good indicators of the efficiency of plant growth and metabolism. Utilising the different neutron cross-sections of H_2O and D_2O a method for visualizing water uptake in plants has been developed [13]. In an experiment performed at CONRAD, rose plants were watered with D_2O at some point in time and neutron radiographs of the plants were taken at regular time intervals afterwards; see Fig. 5.

References

1. A. Hilger, N. Kardjilov, M. Strobl, W. Treimer, J. Banhart, Physica B **385–386** (2006), S. 1213–1215.
2. S. Vogel, PhD. Thesis, available online at http://eldiss.uni-kiel.de/macau/receive/dissertation_diss_00000330 (2000).

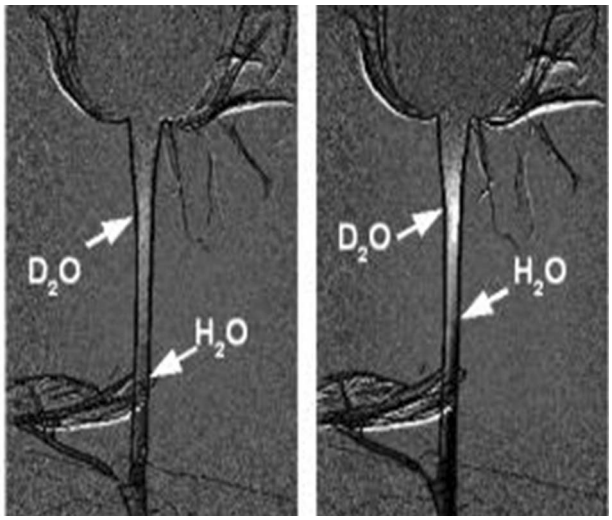

Figure 5. Uptake of D_2O and H_2O in 'Red Giant' rose samples at 10 min (left) and 30 min (right) after D_2O supply.

3. N. Kardjilov, A. Hilger, I. Manke, F. Garcia-Moreno, J. Banhart, *MP Materials Testing* **50**, p. 569–571 (2008).
4. W. Treimer, M. Strobl, N. Kardjilov, A. Hilger, I. Manke, *Applied Physics Letters* **89**, 203504 (2006).
5. W. Kockelmann, G. Frei, E.H. Lehmann, P. Vontobel, J.R. Santisteban, *Nucl. Instr. and Meth*. A **578**, 421–434 (2007).
6. J. R. Santisteban, L. Edwards, A. Steuwer, P. J. Withers, *J. Appl. Cryst*. **34**, 289–297 (2001).
7. A. Steuwer, J. R. Santisteban, P. J. Withers, L. Edwards, M. E. Fitzpatrick, M. R. Daymond, G. Bruno,. *Stat. Solidi* (a) **185**, 221–230 (2001).
8. N. Kardjilov, I. Manke, M. Strobl, A. Hilger, W. Treimer, M. Meissner, T. Krist, J. Banhart, *Nature Physics* **4**, 399–403 (2008).
9. I. Manke, N. Kardjilov, M. Strobl, A. Hilger, J. Banhart, *Journal of Applied Physics*, **104**, 076109 (2008).
10. N. Kardjilov, I. Manke, A. Hilger, M. Dawson, J. Banhart, *Advanced Materials & Processes Magazine* **166**, p. 43–44 (2008).
11. Th. Krist, S. J. Kennedy, T. J. Hick, F. Mezei, *Physica B* **241–243**, 82–85 (1998).
12. I. Manke, Ch. Hartnig, M. Gruenerbel, J. Kaczerowski, W. Lehnert, N. Kardjilov, A. Hilger, J. Banhart, W. Treimer, M. Strobl, *Applied Physics Letters* **90**, 184101 (2007).
13. U. Matsushima, W.B. Herppich, N. Kardjilov, W. Graf, A. Hilger, I. Manke, *Nucl. Instr. and Meth*. A, submitted.